

Kinetics and Equilibrium of Age-Induced Precipitation in Cu-4 At. Pct Ti Binary Alloy



SATOSHI SEMBOSHI, SHINTARO AMANO, JIE FU, AKIHIRO IWASE,
and TAKAYUKI TAKASUGI

Transformation kinetics and phase equilibrium of metastable and stable precipitates in age-hardenable Cu-4 at. pct Ti binary alloy have been investigated by monitoring the microstructural evolution during isothermal aging at temperatures between 693 K (420 °C) and 973 K (700 °C). The microstructure of the supersaturated solid solution evolves in four stages: compositional modulation due to spinodal decomposition, continuous precipitation of the needle-shaped metastable β' -Cu₄Ti with a tetragonal structure, discontinuous precipitation of cellular components containing stable β -Cu₄Ti lamellae with an orthorhombic structure, and eventually precipitation saturation at equilibrium. In specimens aged below 923 K (650 °C), the stable β -Cu₄Ti phase is produced only due to the cellular reaction, whereas it can be also directly obtained from the intergranular needle-shaped β' -Cu₄Ti precipitates in specimens aged at 973 K (700 °C). The precipitation kinetics and phase equilibrium observed for the specimens aged between 693 K (420 °C) and 973 K (700 °C) were characterized in accordance with a time-temperature-transformation (TTT) diagram and a Cu-Ti partial phase diagram, which were utilized to determine the alloy microstructure, strength, and electrical conductivity.

DOI: 10.1007/s11661-016-3949-x

© The Minerals, Metals & Materials Society and ASM International 2017

I. INTRODUCTION

AMONG various Cu-based alloys, age-hardenable Cu-Ti alloys are characterized by superior mechanical strength, stiffness, stress-relaxation, and electrical conductivity properties. In particular, Cu-Ti alloys containing 1 to 6 at. pct Ti exhibit effective precipitation-hardening behavior, while alloys with 4.0 to 4.2 at. pct Ti are widely used for commercial manufacturing because of their excellent mechanical properties and good workability. Therefore, numerous fundamental and applied studies of age-hardenable Cu-Ti alloys have been actively reported since the 1970s.^[1–18]

Alloys are typically manufactured through solid-solution treatment at around 1123 K (850 °C) followed by aging at medium temperatures between 673 K (400 °C) and 773 K (500 °C). The alloy microstructure evolves during isothermal aging *via* the following subsequent processes: compositional modulation of the parent supersaturated Cu solid solution, continuous nucleation and growth of fine needle-shaped precipitates, and discontinuous precipitation of laminated cellular

components at the grain boundaries.^[1–6,12,19] The observed crystallographic features revealed that compositional modulation occurred due to the spinodal decomposition of the α phase of the Cu solid solution, which resulted in the formation of the Ti-lean and Ti-rich fcc disordered regions along the $\langle 100 \rangle$ direction.^[1–6,12,19–22] The fine needle-shaped precipitates are produced due to the transformation of the Ti-rich fcc disordered regions into coherent metastable ordered β' -Cu₄Ti phases with the orientation relationships between the matrix and the precipitate species of $(001)_{\alpha} // (001)_{\beta'}$, $[310]_{\alpha} // [100]_{\beta'}$, and $[130]_{\alpha} // [010]_{\beta'}$.^[1–6,10,12,19–24] In these studies, the β' -Cu₄Ti phase was characterized by a body-centered tetragonal structure (prototype: Ni₄Mo, spacing group: $I4/m$) with lattice parameters of $a = 0.586$ nm and $c = 0.365$ nm. The cellular components were composed of the depleted Cu (α') solute and stable β -Cu₄Ti laminates, which were formed due to the reaction $\alpha \rightarrow \alpha' + \beta$ -Cu₄Ti at the grain boundaries, with orientation relationships of $(111)_{\alpha} // (010)_{\beta}$ and $[\bar{1}10]_{\alpha} // [001]_{\beta}$.^[12,19,25–28] The β -Cu₄Ti crystal structure was an orthorhombic one (prototype: Au₄Zr; spacing group: $Pnma$) with lattice parameters of $a = 0.453$ nm, $b = 0.434$ nm, and $c = 1.292$ nm. On the other hand, it has been reported that Widmanstätten microstructures appear during aging at high temperatures above 973 K (700 °C) or 1013 K (740 °C), although the details of the high-temperature microstructural evolution still remain somewhat controversial.^[9,12,26,29–31]

It is generally accepted that the microstructure of aged Cu-Ti alloys is closely related to their mechanical and physical properties. For example, the strength of

SATOSHI SEMBOSHI is with the Institute for Materials Research (Trans-Regional Corporation Center for Industrial Materials Research), Tohoku University, Gakuen-cho 1-1, Naka-ku, Sakai, Osaka 599-8531, Japan. Contact e-mail: semboshi@imr.tohoku.ac.jp SHINTARO AMANO, AKIHIRO IWASE, and TAKAYUKI TAKASUGI are with the Department of Materials Science, Osaka Prefecture University, Gakuen-cho 1-1, Naka-ku, Sakai, Osaka 599-8531, Japan JIE FU is with the Research Organization for the 21st Century, Osaka Prefecture University, Gakuen-cho 1-1, Naka-ku, Sakai, Osaka 599-8531, Japan.

Manuscript submitted May 15, 2016.

Article published online January 12, 2017

Cu-Ti alloys increases with continuous nucleation and growth of the needle-shaped fine β' -Cu₄Ti precipitates.^[6–19] On the other hand, the alloy strength decreases during prolonged aging, which is caused by the development of discontinuous coarse cellular precipitates containing stable β -Cu₄Ti laminates instead of β' -Cu₄Ti hardening species.^[19] Thus, understanding the microstructural evolution (precipitation behavior) of the alloys is important for controlling their properties. The objective of this study was to investigate the microstructural evolution of commercial Cu-4 at. pct Ti alloy during isothermal aging in the wide temperature range between 693 K (420 °C) and 973 K (700 °C) through constructing time–temperature–transformation (TTT) and revised partial phase diagrams. Based on the obtained results, the transformation kinetics and phase equilibrium of the age-induced precipitates as well as the relationship between the alloy microstructure and properties (such as electrical conductivity and hardness) have been discussed.

II. EXPERIMENTAL

Commercial age-hardenable Cu-Ti alloy with a chemical Ti concentration of 4.04 at. pct was provided by DOWA METALTECH Co., Ltd. An alloy ingot was prepared by melting the raw materials [namely, pure Cu (99.99 wt pct) and Ti (99.99 wt pct)] under Ar gas atmosphere, hot-rolling the resulting melt to a thickness of 0.22 mm at 1223 K (950 °C), and finally quenching it in water to produce the supersaturated α phase. Strip-like specimens with dimensions of 60 mm \times 6 mm were cut from the obtained sheet using a shearing machine. A contaminated layer was removed from the sample surface by mechanical grinding. Some of the produced specimens were isothermally aged at temperatures of 693 K (420 °C), 723 K (450 °C), and 773 K (500 °C) inside quartz capsules evacuated to pressures below 2.0×10^{-3} Pa. The remaining specimens were isothermally aged at 873 K (600 °C), 923 K (650 °C), and 973 K (700 °C) inside the salt bath composed of a mixture of BaCl₂, CaCl₂, and NaCl reagents.

The microstructures of the aged specimens were observed using a JEOL JSM-7001F field emission scanning electron microscopy (FESEM) system operated at a voltage of 15 kV and a JEOL JIM-3010 transmission electron microscopy (TEM) instrument operated at a voltage of 300 kV. To obtain FESEM microstructural images, the specimens were mechanically polished using 2000-grade emery paper and then chemically etched with a 7 mol/L nitric acid solution at 273 K (0 °C) for 10 seconds. To obtain TEM images, thin foil-like specimens were ground to thicknesses below 30 μ m and then subjected to low-angle ion milling using an Ar ion beam accelerated at voltages below 3 kV. High-purity (99.9999 mass pct) Ar gas was used as the Ar ion-beam source. Volume fractions of the cellular components (containing the depleted Cu (α') solute and β -Cu₄Ti lamellae) were obtained from the FESEM images analyzed by a point count method implemented into the Acrobat Photoshop CS software. In order to

obtain statistically accurate volume fraction values, larger regions (with sizes greater than 12,000 μ m²) were analyzed using more than 10 FESEM images obtained at magnifications of 2000.

Age-induced precipitates, such as Ti-rich disordered fcc particles, β' -Cu₄Ti needles, and β -Cu₄Ti lamellae, were separated from the specimens using the extraction procedure described in previous studies.^[19,32] First, the surfaces of the aged alloy specimens were ground to remove contaminated layers. Afterwards, the specimens were cut into smaller pieces, which could be effectively dissolved in solution. These pieces were immersed in a 7 mol/L nitric acid solution at 273 K (0 °C) and stirred in an ultrasonic bath for approximately 20 minutes. After the Cu solid solution phase in the pieces was dissolved by the acid, the remaining precipitates were separated using a membrane filter with a pore diameter of 50 nm, thoroughly rinsed with pure water, and dried in a desiccator. The resulting filtrate and washing solution were collected in a beaker that contained a 9 mol/L sulfuric acid solution to prevent the hydrolysis of Ti species during filtration. The crystal structure of the separated precipitates was analyzed *via* X-ray diffraction (XRD) using a PANalytical X'pert Pro diffractometer with CuK α radiation at an applied voltage of 40 kV. The mass fractions of the elemental Cu and Ti in the precipitate and matrix phases separated from the aged specimen *via* extraction were analyzed through inductively coupled plasma-optical emission spectrometry (ICP-OES) using a Thermo Fisher Scientific IRIS Advantage DUO instrument.^[19,32,33]

The microstructural evolution of the specimens during aging was monitored by measuring their electrical conductivity and Vickers hardness. The electrical conductivity of the aged specimens with lengths of 60 mm was measured by a constant DC-current four-probe method of the Agilent 34420A micro-ohm meter at a temperature of 293 K (20 °C) and current of 100 mA. The Vickers hardness of the aged samples was evaluated using an AKASHI MVK-E Vickers microhardness tester at an applied load of 4.9 N and testing duration of 10 seconds. The hardness values were obtained by averaging the results of 12 indentations (after excluding the maximum and minimum values).

III. RESULTS AND DISCUSSION

A. Microstructural Evolution

1. Alloy specimens aged between 693 K (420 °C) and 923 K (650 °C)

The as-quenched Cu-Ti alloy specimens contained a single phase of the supersaturated Cu solid solution α with an average grain size of 30 μ m. Figure 1 shows the microstructural evolution of the specimens aged at 723 K (450 °C). The TEM image of the specimen aged for 60 minutes (1 hour; see Figure 1(a)) is characterized by typical high-contrast wavy and modulated coherent strain features, owing to the decomposition of the supersaturated parent α phase into disordered Ti-lean and Ti-rich fcc α particles with sizes of several

nanometers. This image is similar to those previously obtained for Cu-Ti dilute alloys, which were aged for a shorter period.^[1-6,10] According to the results of the selected area electron diffraction (SAED) studies displayed in the inset of Figure 1(a), only fundamental reflections corresponding to the fcc structure were detected, indicating that aging for 60 minutes has not led to the formation of the ordered metastable β' -Cu₄Ti precipitates. For the specimen aged for 180 minutes (3 hours; see Figure 1(b)), fine needle-shaped precipitates with lengths of several tens of nanometers were dispersed homogeneously in the grains. The structure of these precipitates corresponded to ordered metastable β' -Cu₄Ti species, as indicated by the weak super-lattice reflections of the previously reported SAED patterns.^[1-6] The needle-shaped β' -Cu₄Ti precipitates continuously nucleated during prolonged aging in the disordered Ti-rich fcc regions and grew until reaching maximum lengths of approximately 100 nm, as shown in the inset of Figure 1(c). In addition, cellular components were formed discontinuously at the grain boundaries during aging (as arrowed in Figure 1(c)). The development of cellular components was accompanied by the consumption of the needle-shaped β' -Cu₄Ti precipitates. Ultimately, only the cellular components were observed inside the specimen, which had been aged for 28,800 minutes (480 hours; see Figure 1(d)). As indicated by the corresponding SAED pattern depicted in the inset of Figure 1(d), these cellular components were composed of the Cu solid solution α' and stable β -Cu₄Ti lamellae. No apparent microstructural evolution could be observed at prolonged aging periods greater than 480 hours, which indicated that the specimens almost reached an equilibrium state.

The same microstructural evolution characteristics, which include the decomposition into the disordered Ti-lean and Ti-rich fcc α phases, continuous precipitation of the needle-shaped fine β' -Cu₄Ti, discontinuous precipitation of the coarse cellular components composed of α' and β -Cu₄Ti lamellae, and eventual occupation of the entire specimen with cellular components were also observed for the specimens aged at temperatures between 693 K (420 °C) and 923 K (650 °C). Figure 2 representatively shows the microstructural evolution of the specimens aged at 923 K (650 °C). Naturally, the initiation kinetics of the metastable needle-shaped β' -Cu₄Ti precipitates and stable lamellar β -Cu₄Ti cellular components was accelerated by increasing aging temperature, which will be discussed in detail in the next sections.

2. Alloy specimens aged at 973 K (700 °C)

Figure 3 shows the microstructural evolution of the specimens aged at 973 K (700 °C). During the early aging stages (<0.2 minutes) depicted in Figure 3(a), only the fine needle-shaped precipitates, which were similar to those detected for the specimens aged below 923 K (650 °C) (see Figures 1(b) and 2(a)), were formed homogeneously in the grain interiors. However, after aging for 1 minute, the observed microstructural features were apparently different from those of the specimens aged below 923 K (650 °C) (see Figures 1(c),

(d) and 2(b), (d)). In particular, the needle-shaped precipitates significantly coarsened, reaching sizes above 100 nm, and then grew up to more than 1 μ m in length after aging for 20 minutes (in comparison, the maximum length of the precipitate particles in the specimens aged at temperatures below 923 K (650 °C) was several hundred nanometers, as indicated by Figure 2(b)). In addition, the coarse intergranular plates (marked by the arrows in Figures 3(b) through (d)) together with the cellular components (marked by the dotted circles) were detected at the grain boundaries. After aging for more than 20 minutes, the microstructural evolution reached saturation, as shown in Figure 3(d), when both the intragranular needle-shaped precipitates and intergranular plates grew without replacement with cellular components as observed during aging at temperatures below 923 K (650 °C). Similar microstructures corresponding to a mixture of the “pearlite”- and “Widmanstätten”-type precipitates were observed for Cu-3 to 4.3 wt pct Ti alloys aged at 1023 K (750 °C).^[26-31] The former precipitates correspond to cellular components, while the latter precipitates represent intergranular plates.

The precipitate structures obtained for the specimens aged at 973 K (700 °C) were examined by the TEM-SAED and XRD techniques after the extraction procedure.^[19,32] The obtained TEM-SAED patterns corresponding to the needle-shaped β' -Cu₄Ti precipitates were observed for the specimen aged for less than 2 minutes, whereas after aging for 5 minutes, both the β' -Cu₄Ti and β -Cu₄Ti phases of the needle-shaped precipitates were detected, suggesting continuous precipitation of the needle-shaped species due to the transformation of β' -Cu₄Ti into β -Cu₄Ti. Figure 4 shows the XRD profile of the precipitates extracted from the specimen, which was aged at 973 K (700 °C) for 40 minutes (during the final aging stage). All the detected XRD peaks correspond to the orthorhombic β -Cu₄Ti,^[23,24] indicating that all precipitates, such as intragranular needles, intergranular plates, and cellular laminates, possess the same crystal structure of orthorhombic β -Cu₄Ti.

To briefly summarize the observed microstructural evolution, the structure of the age-induced precipitates undergoes transformation in accordance with the following sequence: a disordered Ti-rich fcc phase, metastable tetragonal β' -Cu₄Ti, and stable orthorhombic β -Cu₄Ti, which is common for the specimens aged at temperatures between 693 K (420 °C) and 973 K (700 °C). On the other hand, the resulting microstructure of the specimens aged for a prolonged period below 923 K (650 °C) and above 973 K (700 °C) is completely different, which suggests that the dominant diffusion mode of the solute atoms changes from the grain boundary diffusion below 923 K (650 °C) to the bulk diffusion above 973 K (700 °C). During aging below 923 K (650 °C), the stable β -Cu₄Ti species nucleate and grow due to the reaction at the grain boundaries because the migration of the solute atoms is controlled by the grain boundary diffusion. Therefore, the cellular components containing β -Cu₄Ti laminates develop at the grain boundaries during aging and eventually occupy the entire specimen. However, during aging above 973 K

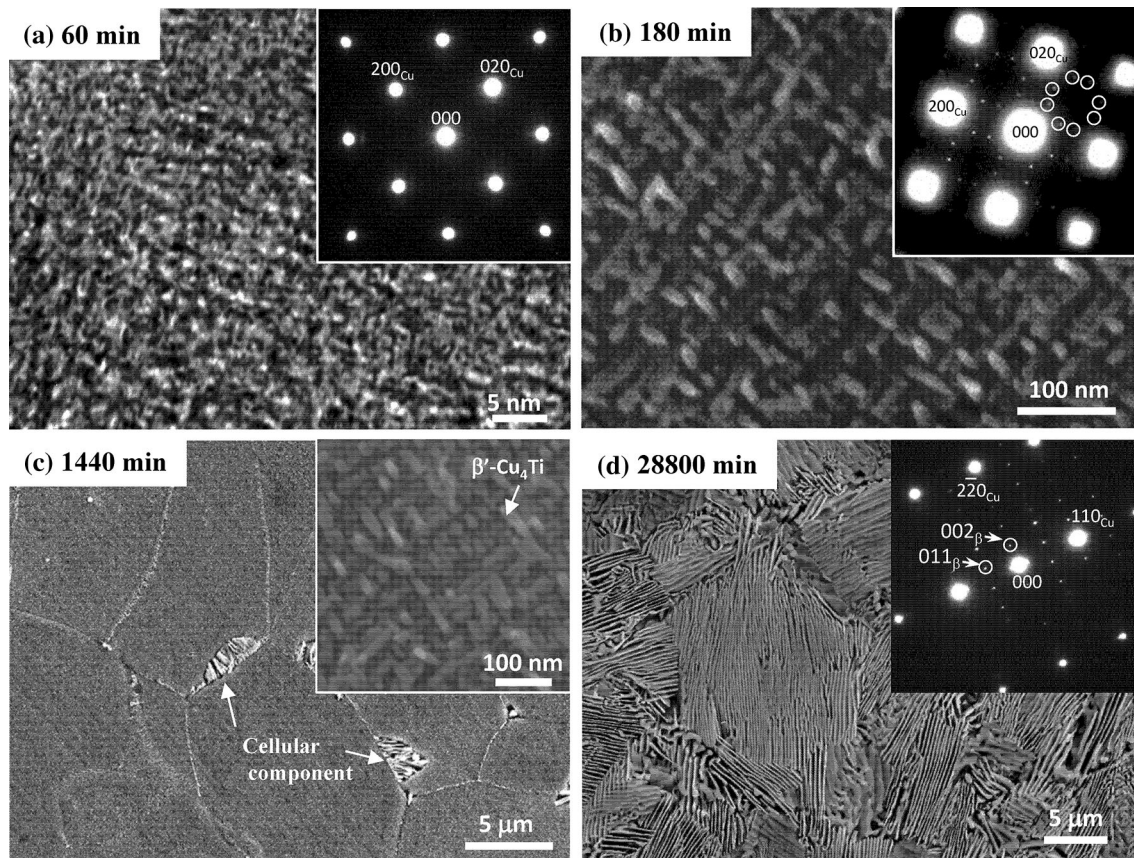


Fig. 1—Micrographs of the Cu-4 at. pct Ti alloy specimens aged at 723 K (450 °C) for (a) 60 minutes, (b) 180 minutes, (c) 1440 minutes, and (d) 28,800 minutes. The insets contain the corresponding SAED patterns (panels (a), (b), and (d)) and FESEM image (panel (c)). The open circles in the SAED pattern of panel (b) indicate the super-lattice reflections from the β' -Cu₄Ti phase with a tetragonal structure. The super-lattice reflections in the SAED pattern of panel (d) were indexed by the β' -Cu₄Ti phase with an orthorhombic structure. The images were obtained at magnifications of (a) 200,000 (TEM) and (b) 100,000, (c) 3000 (50,000 for the inset), and (d) 2000 (FESEM).

(700 °C), the stable β -Cu₄Ti precipitates can be directly produced from the pre-existing β' -Cu₄Ti precipitates and rapidly grow since bulk diffusion dominates at high temperatures. The stable β -Cu₄Ti precipitates can also nucleate at the grain boundaries during aging at high temperatures and grow due to the supply of the solute species from all directions, resulting in the formation of not only cellular components, but also intergranular β -Cu₄Ti plates. Similar results were reported by Doi [29], although in his work, the structure of the stable precipitates was identified as Cu₃Ti derivatives with a close-packed hexagonal lattice.

B. Precipitation Kinetics

Using the results of the microstructural evolution described earlier, a time-temperature-transformation (TTT) diagram was constructed for Cu-4 at. pct Ti alloy. The kinetics of the transformation from disordered fcc Ti-rich particles into ordered metastable tetragonal β' -Cu₄Ti precipitates was examined by identifying super-lattice β' -Cu₄Ti reflections of the obtained TEM-SAED patterns. For example, super-lattice reflections were not detected for the specimen aged for 60 minutes at 723 K (450 °C); however, they were

observed for the specimen aged for 180 minutes at the same temperature, as shown in Figures 1(a) and (b). In this work, volume fractions of the constituent precipitates were determined quantitatively *via* Rietveld fitting of the XRD profiles of the insoluble precipitates separated during the extraction procedure. Figure 5 displays the precipitate volume fraction plotted as a function of aging time for the specimen aged at 723 K (450 °C), which has been reported earlier.^[19] According to Figure 5, the volume fraction of β' -Cu₄Ti in the specimen aged for 180 minutes was approximately 0.2 vol pct. Therefore, it can be concluded that the TEM-SAED detection limit for β' -Cu₄Ti species is approximately 0.2 vol pct.

Super-lattice reflections displayed in the TEM-SAED patterns were actually detected for the specimens aged at 693 K (420 °C) for 720 minutes, 723 K (450 °C) for 180 minutes, 773 K (500 °C) for 30 minutes, 873 K (600 °C) for 1 minutes, 923 K (650 °C) for 0.25 minutes, and 973 K (700 °C) for 0.1 minute. Figure 6 shows the Arrhenius plots describing the initiation of the ordered β' -Cu₄Ti precipitates. The obtained data points are plotted on a straight line in the temperature region between 693 K (420 °C) and 973 K (700 °C), which corresponds to the following equation:

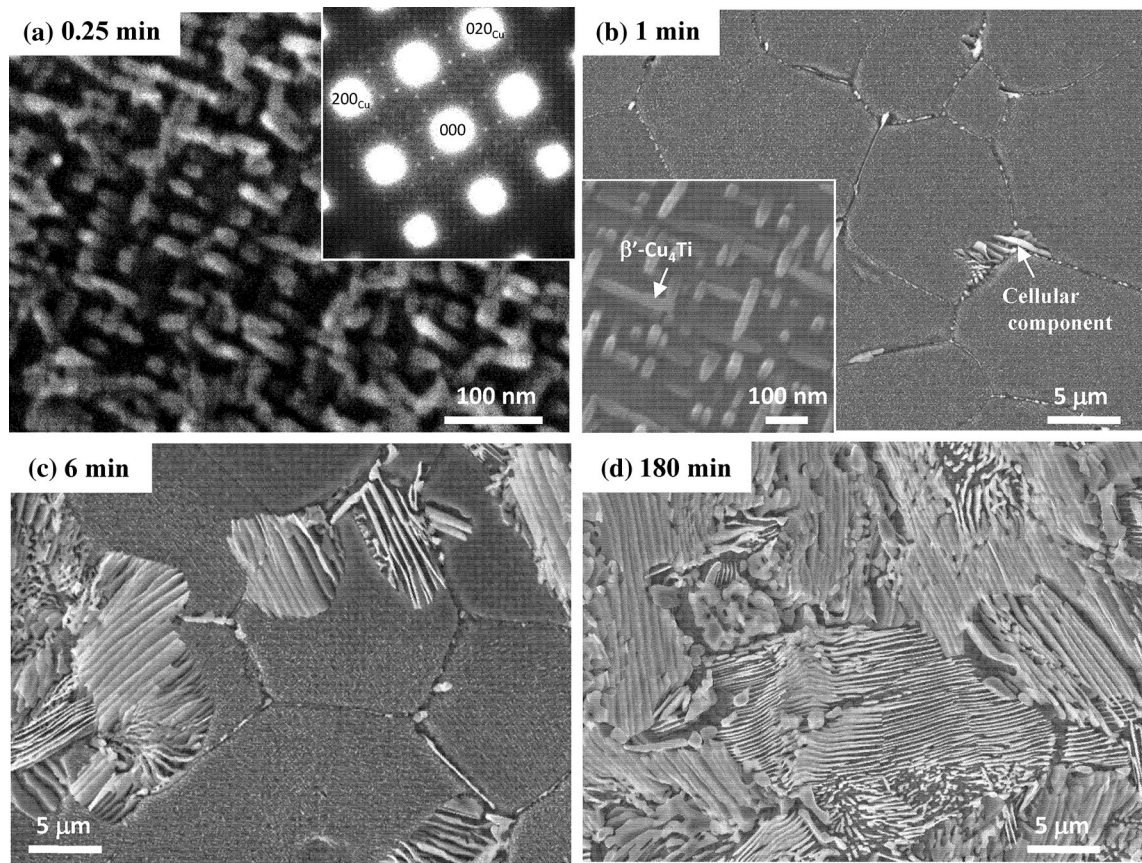


Fig. 2—Micrographs of the Cu-4 at. pct Ti alloy specimens aged at 923 K (650 °C) for (a) 0.25 minutes, (b) 1 minute, (c) 6 minutes, and (d) 180 minutes. The insets contain the corresponding SAED patterns (panels (a)) and FESEM image (panel (b)). The FESEM images were obtained at magnifications of (a) 100,000 and (b) through (d) 2000 (50,000 for the inset of (b)).

$$\ln(t) = -25.3 + 22.0 \times 10^3/T, \quad [1]$$

where t is the aging time (minutes) and T is the aging temperature (K). The equation approximately describes the initiation kinetics of β' -Cu₄Ti.

The kinetics of the initiation and saturation of the stable orthorhombic β -Cu₄Ti precipitates was evaluated for the specimens aged below 923 K (650 °C). The initiation and saturation stage for the stable orthorhombic β -Cu₄Ti species were determined from the volume fractions of the cellular components (obtained from the FESEM images) plotted vs aging time. Figure 7(a) shows the volume fractions of the cellular components V_c plotted for the specimens aged between 693 K (420 °C) and 923 K (650 °C) as functions of the aging time. Note that it was difficult to quantitatively determine the volume fraction of stable β -Cu₄Ti in the specimen aged at 973 K (700 °C) from the corresponding FESEM image because stable β -Cu₄Ti species could be initiated not only *via* a cellular reaction, but also due to the direct intragranular transformation of the pre-existing needle-shaped precipitates. Figure 7(a) indicates that the V_c of the cellular components increases sigmoidally with increasing aging time regardless of the aging temperature, while Figure 7(b) depicts the V_c values plotted as $\ln[-\ln(1 - V_c)]$ vs $\ln(t)$ (a so-called “Johnson–Mehl–Avrami plot”). The plots obtained for each aging

temperature can be fitted with a linear approximation, which allows calculation of the constants A and B of the Johnson–Mehl–Avrami equation (defined by the formula $\ln[-\ln(1 - V_c)] = A + B \ln(t)$; see Table I). Thus, the values of the aging time t corresponding to the initiation and saturation stages of the β -Cu₄Ti formation were defined at V_c values of 5 and 95 pct, respectively. The obtained magnitudes were also plotted in Figure 6 and fitted using the following equations:

$$\beta - \text{Cu}_4\text{Ti initiation} : \ln(t) = -21.3 + 20.1 \times 10^3/T \quad [2]$$

$$\beta - \text{Cu}_4\text{Ti saturation} : \ln(t) = -21.7 + 22.1 \times 10^3/T \quad [3]$$

Figure 8 shows the TTT diagram constructed for the Cu-4 at. pct Ti alloy, in which the kinetics of the β' -Cu₄Ti initiation, β -Cu₄Ti initiation, and β -Cu₄Ti saturation could be described by Eqs. [1], [2], and [3], respectively. The obtained data reveal that the microstructural evolution during isothermal aging can be apparently divided into the following four regions on the TTT diagram: [I] the supersaturated α phase decomposes spinodally into the Ti-rich and Ti-lean fcc

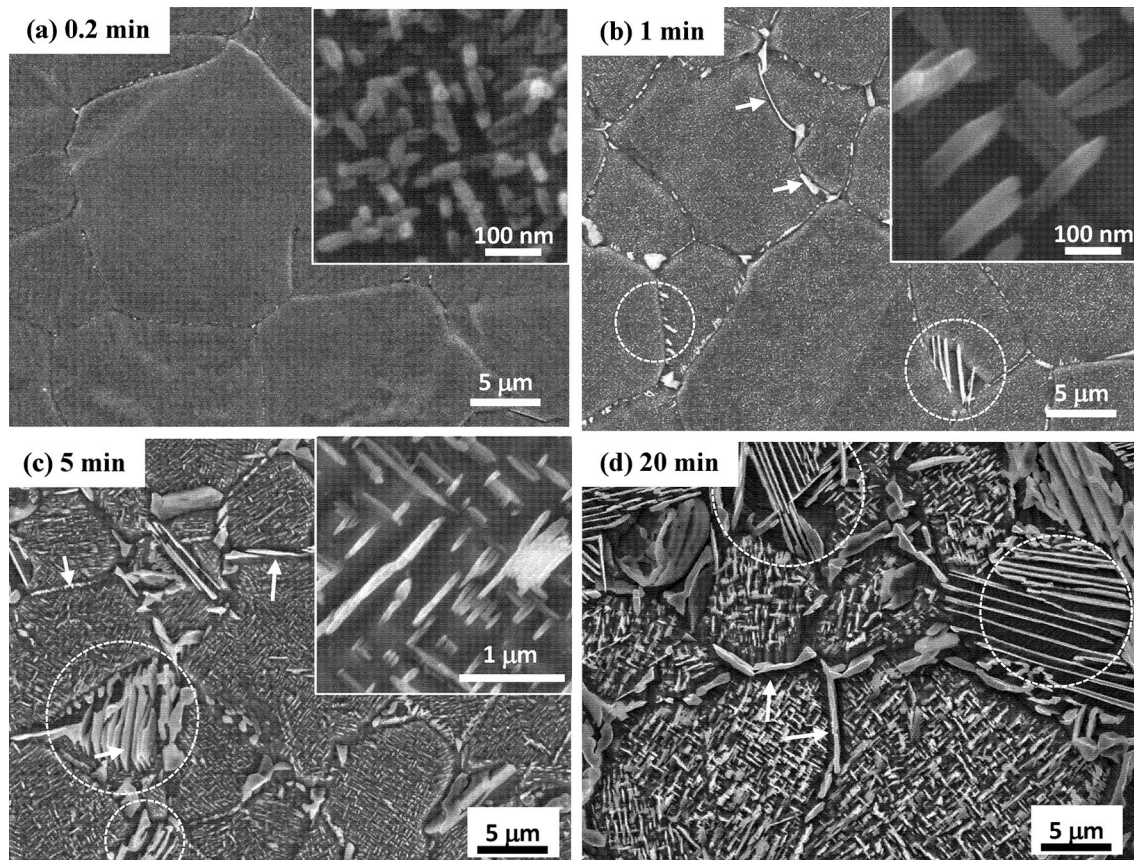


Fig. 3—Micrographs of the Cu-4 at. pct Ti alloy specimens aged at 973 K (700 °C) for (a) 0.2 minutes, (b) 1 minute, (c) 5 minutes, and (d) 20 minutes, which were obtained by FESEM at a magnification of 2000. The images obtained by FESEM at higher magnifications of (a) 80,000, (b) 80,000, and (c) 15,000 are shown in the corresponding insets. The dotted circles in panels (b), (c), and (d) denote the cellular components, while the solid arrows designate the intergranular plates.

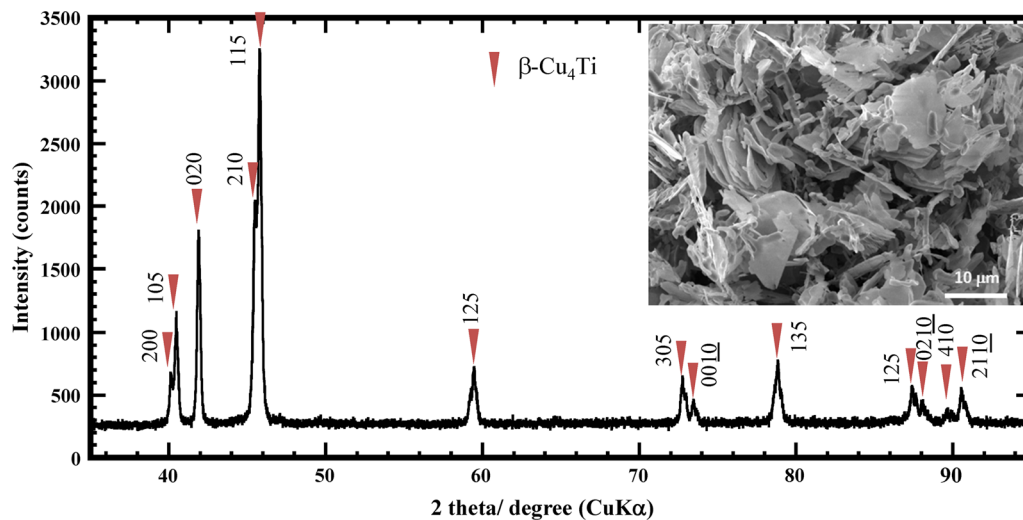


Fig. 4—An XRD pattern recorded for the precipitates in the Cu-4 at. pct Ti alloy specimen aged at 973 K (700 °C) for 40 minutes, which were extracted by treatment with a 7.0 mol/L nitric acid solution (the corresponding FESEM image is shown in the inset).

phases; [II] the Ti-rich fcc regions are continuously transformed into the ordered tetragonal β' -Cu₄Ti phases; [III] the tetragonal β' -Cu₄Ti species continue to grow, and stable orthorhombic β -Cu₄Ti is also formed; and [IV] the metastable tetragonal β' -Cu₄Ti species disappear,

leaving only stable β -Cu₄Ti precipitates dispersed in the alloy matrix. Since no more microstructural changes occurred in region [IV], it can be suggested that the specimen has finally reached an equilibrium state. The described microstructural evolution was accelerated

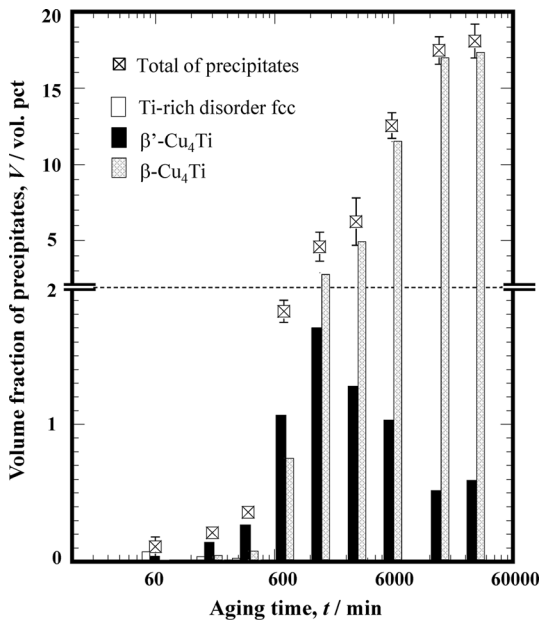


Fig. 5—Volume fractions of the precipitates formed in the Cu-4 at. pct Ti alloy specimens during aging at 723 K (450 °C), which was reprinted from the reference of Ref. [19].

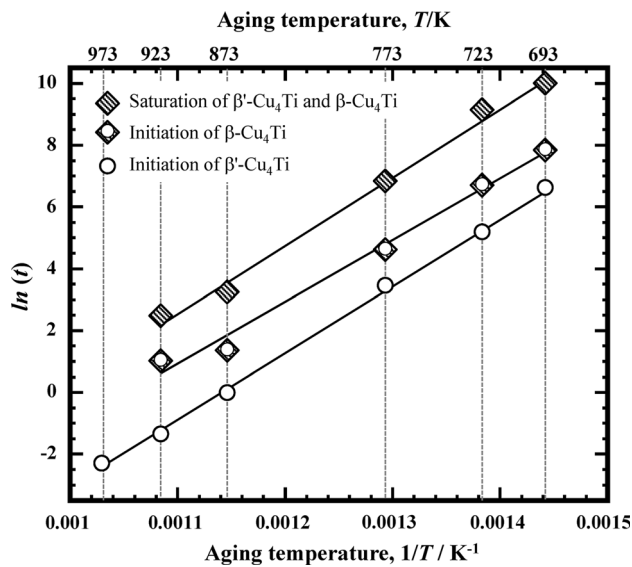


Fig. 6—Arrhenius plots of the aging time (represented by $\ln(t)$) vs aging temperature, which describe the β' - Cu_4Ti precipitation initiation and the formation and saturation of cellular components (containing β - Cu_4Ti) in the Cu-4 at. pct alloy specimens. The last two processes correspond to the volume fractions of the cellular components equal to 5 and 95 pct, respectively, which were calculated using the Johnson–Mehl–Avrami equation.

exponentially by the increase in the aging temperature in accordance with the Arrhenius equation.

C. Phase Equilibrium

According to the Gibbs phase rule, when a binary alloy contains two phases in an equilibrium state at a temperature, the composition and volume fraction of

each phase are fixed. The TTT phase diagram depicted in Figure 8 indicates that the specimens aged under the conditions specified in region [IV] contained only the terminal α and β - Cu_4Ti phases. In addition, the volume fractions of both phases in region [IV] were approximately constant during isothermal aging over a prolonged period, because no significant microstructural changes occurred. Therefore, the specimens isothermally aged in region [IV] appeared to be in an equilibrium state, as will be discussed in the next section.

Table II lists the composition and volume fractions of both the α and β - Cu_4Ti constituent phases for the specimens in the equilibrium state, which were analyzed using the extraction procedure combined with ICP-OES measurements.^[19,32] In order to convert mass fractions into the corresponding volume fractions, the ideal alloy densities of 8.9 and 7.9 g/cm³ were utilized for the α and β - Cu_4Ti constituent phases, respectively.^[23] The amounts of Ti in the Cu solid solution and β - Cu_4Ti precipitation phases of the specimens in the equilibrium state (denoted as $C_{\text{Ti eq}}^{\alpha}$ and $C_{\text{Ti eq}}^{\beta}$, respectively) can be fitted with the linear functions plotted in Figure 9, which are described by the following equations:

$$\ln C_{\text{Ti eq}}^{\alpha} = 0.22 - 3.99 \times 10^3 / T \quad [4]$$

$$\ln C_{\text{Ti eq}}^{\beta} = -1.39 - 0.14 \times 10^3 / T \quad [5]$$

The magnitudes of $C_{\text{Ti eq}}^{\alpha}$ and $C_{\text{Ti eq}}^{\beta}$ correspond to the terminal composition of Ti in the two-phase region. Therefore, we can propose a Cu-Ti partial phase diagram (solid lines) depicted in Figure 10, which was constructed after taking into account the recent phase diagram created by Turchanin *et al.* from the thermodynamic assessment obtained by the CALPHAD approach (dotted lines).^[34] Numerous studies on stable phase transformations in the Cu-Ti system have been reported,^[11,25,35–40] which were reviewed by Turchanin *et al.*^[34] Brun *et al.* proposed an experimental phase diagram including two modifications of the β' - and β - Cu_4Ti phases with a peritectoid transformation between them at 773 K (500 °C).^[40] However, since the β' - Cu_4Ti phase is metastable (as confirmed in this study), it will not be taken into account. The composition of the β - Cu_4Ti precipitates obtained in this study ($C_{\text{Ti eq}}^{\beta}$) was very close to the ideal stoichiometric composition of 20 at. pct Ti, which was in good agreement with the results of the XRD and TEM-EDS measurements^[31,38,40] (in contrast to the data reported by Karlsson,^[41] which suggested that the composition of the Cu-richest intermetallic compound was Cu_3Ti). The terminal composition obtained for β - Cu_4Ti via Eq. [5] agrees well with the range reported earlier (between 19.1 and 20.2 at. pct) within experimental accuracy.^[25,37,38,40] The obtained terminal composition of the $C_{\text{Ti eq}}^{\alpha}$ phase (solidus line) was shifted left with respect to the magnitude depicted in the recent diagram, although some previously reported experimental data were closer to the value of $C_{\text{Ti eq}}^{\alpha}$ determined in this study.^[11,35,40]

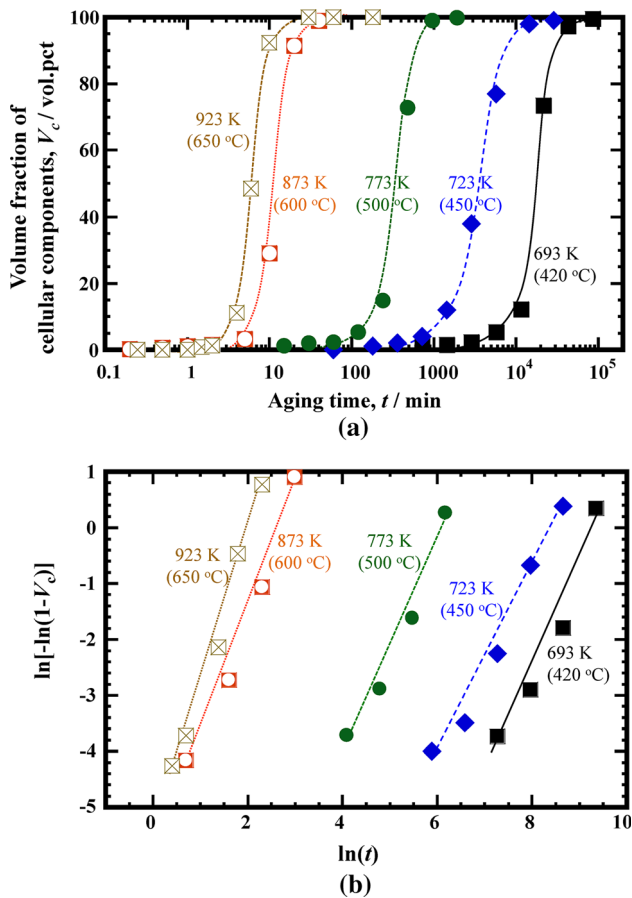


Fig. 7—Volume fractions of the cellular components in the Cu-4 at.pct alloy specimens aged at 693 K (420 °C), 723 K (450 °C), 773 K (500 °C), 873 K (600 °C), and 923 K (650 °C), which are plotted as (a) volume percentages vs aging time (in minutes) and (b) $\ln[-\ln(1 - V_c)]$ vs $\ln(t)$.

D. Effect of Microstructural Evolution on Alloy Properties

Figure 11 shows the electrical conductivity and Vickers hardness values for the specimens aged at temperatures between 693 K (420 °C) and 973 K (700 °C) (the electrical conductivity of the as-quenched alloy specimens measured before aging was 4.5 pct of the International Annealed Copper Standard (IACS)*). The

*Electrical conductivity unit corresponding to the conductivity of annealed Cu measured at 298 K (25 °C), ($5.8 \times 10^7 \Omega^{-1} \text{ m}^{-1}$).

specimen conductivity gradually increased with aging time and eventually reached saturation at all temperatures specified in Figure 11(a). The obtained saturation values exceeded 30 pct IACS for the specimens aged at 693 K (420 °C) for more than 43,200 minutes (720 hours) and decreased with an increase in the aging temperature. Correspondingly, the total saturation period was reduced with increasing aging temperature.

The Vickers hardness of the as-quenched specimens was 125 HV. During aging, the Vickers hardness value rapidly increased and reached the maximum followed by

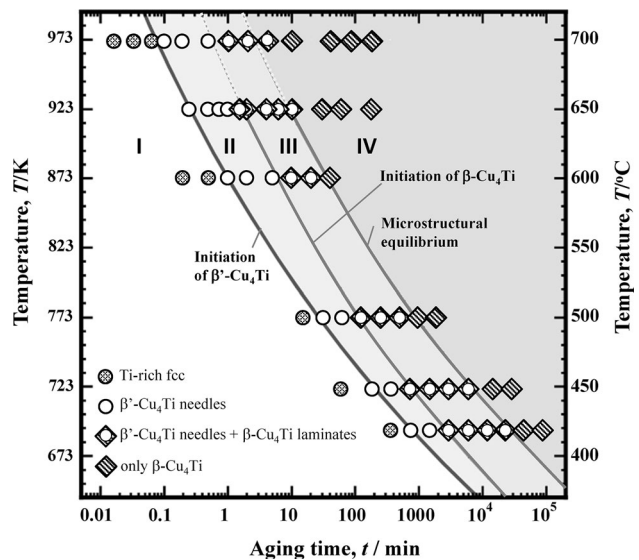


Fig. 8—A TTT diagram constructed for the Cu-4 at.pct Ti alloy specimens. The initiation of the β' - Cu_4Ti precipitation, formation of β - Cu_4Ti species, and microstructural equilibrium are represented by the solid lines. The precipitate structure was evaluated by the FES-EM and TEM-SAED techniques.

a subsequent decrease and saturation, as shown in Figure 11(b). The maximum value of the Vickers hardness decreased with increasing aging temperature, although the aging period required to achieve alloy peak hardening was shortened. The age-hardening behavior of the specimens observed in this work was consistent with the results of the similar studies reported previously.^[6,7,12,19]

Using the data presented in Figure 11, the aging conditions for achieving alloy peak hardness and the electrical conductivity values of 10, 15, 20, and 25 pct IACS are depicted in the TTT diagram, as presented in Figure 12. The electrical conductivity gradually increases during aging from 4.5 pct IACS for the as-quenched state to a saturation value in region [IV], where the alloy microstructure has reached the equilibrium state. The electrical conductivity increase observed for the aged specimens can be primarily explained by the amount of Ti solute in the α phase of the Cu solid solution C_{Ti}^{α} , because the studied specimens were mainly consisted of the α matrix phase (with a volume fraction greater than 80 pct; see Table II). The conductivity of the α phase, $\sigma^{\alpha} [\Omega^{-1} \text{ m}^{-1}]$, has been estimated using the Nordheim equation^[15,42]:

$$1/\sigma^{\alpha} = 1/\sigma_{\text{Cu}} + X C_{\text{Ti}}^{\alpha}, \quad [6]$$

where σ_{Cu} is the electrical conductivity of pure Cu ($\sigma_{\text{Cu}} = 5.8 \times 10^7 \Omega^{-1} \text{ m}^{-1}$, which corresponds to the electrical resistivity of 17.2 n $\Omega \text{ m}$), and the coefficient X is assumed to be equal to 95 n $\Omega \text{ m/at. pct Ti}$.^[15,43] Since the C_{Ti}^{α} decreases during aging due to precipitation of Ti-enriched compounds, the electrical conductivity of the α phase, σ^{α} , increases in accordance with Eq. [6], and eventually the electrical conductivity of the specimen increases as well.

Table I. Calculated Values of Constants A and B of the Johnson–Mehl–Avrami Equation

Aging Temperature, T [K](°C)	A	B
693 K (420 °C)	−18.01	1.92
723 K (450 °C)	−14.17	1.67
773 K (500 °C)	−11.80	1.91
873 K (600 °C)	−5.93	2.19
923 K (650 °C)	−5.54	2.71

Table II. Ti Contents in the Cu Solid Solution ($C_{\text{Ti eq}}^{\alpha}$) and β -Cu₄Ti Phases ($C_{\text{Ti eq}}^{\beta}$), and Volume Fractions of the β -Cu₄Ti Phase (V_f^{β}) in the Fully Aged Cu-Ti Alloy Specimen Obtained After Extraction

Aging Temperature, (Aging Time)	$C_{\text{Ti eq}}^{\alpha}$, At. Pct	$C_{\text{Ti eq}}^{\beta}$, At. Pct	V_f^{β} , Pct
693 K (420 °C), (86,400 minutes)	0.37 ± 0.04	20.4 ± 0.6	18.9
723 K (450 °C), (57,600 minutes)	0.48 ± 0.04	20.5 ± 0.6	18.2
773 K (500 °C), (5760 minutes)	0.82 ± 0.08	20.9 ± 0.8	17.0
873 K (600 °C), (480 minutes)	1.19 ± 0.05	21.4 ± 0.9	15.4
973 K (700 °C), (180 minutes)	2.09 ± 0.06	21.6 ± 1.1	11.0

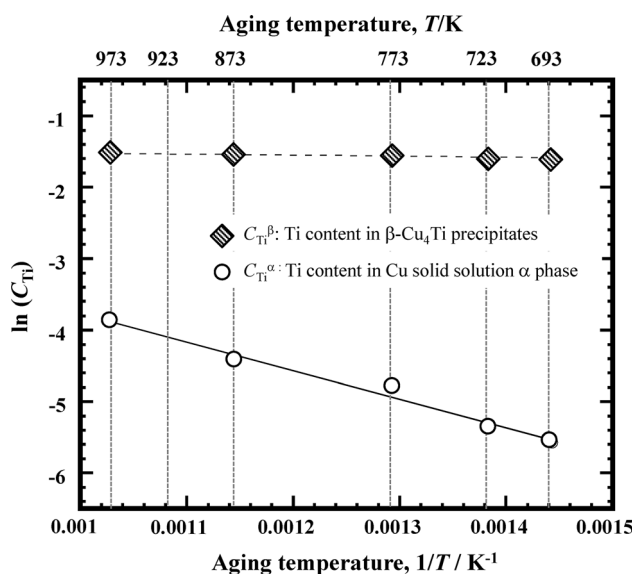


Fig. 9—Ti contents in the Cu solid solution α -phase and β -Cu₄Ti phase of the fully aged Cu-4 at. pct Ti alloy specimens.

The ultimate electrical conductivity of the fully aged alloy increases with decreasing aging temperature as shown in Figures 11 and 12, which can be also explained by the decrease in the terminal composition of the Ti solute in the α phase, $C_{\text{Ti eq}}^{\alpha}$ (as indicated by the phase diagram depicted in Figure 10). Thus, when the aging temperature decreases from 973 K (700 °C) to 693 K (420 °C), the $C_{\text{Ti eq}}^{\alpha}$ value decreases from 2.0 at.pct to 0.38 at.pct according to Eq. [4]. As a result, the electrical conductivity of the α phase, which was calculated using Eq. [6], increased from 8.3 pct IACS to 32 pct IACS. Since the electrical conductivity of the β -Cu₄Ti phase ($0.26 \times 10^7 \Omega^{-1} \text{ m}^{-1}$, which corresponds to the electrical resistivity of 385 n Ωm) is much smaller than that of the α phase,^[7] the electrical conductivity of the fully aged

specimen containing both the α and β -Cu₄Ti phases (σ) can be approximated by the following equation^[44,45]:

$$\sigma^{\alpha} / \sigma \approx 1 + 3/2V_f^{\beta} \quad [7]$$

In this work, the electrical conductivities of the fully aged specimens were calculated using Eq. [7] and the V_f^{β} values listed in Table II. Consequently, it has been shown that the electrical conductivity of the specimen increased from 7.2 to 27 pct IACS, which were close to the experimental values plotted in Figure 11.

In addition, Figure 12 shows that the aging conditions for achieving alloy peak hardness correspond to the initiation of lamellar β -Cu₄Ti cellular components at temperatures below 923 K (650 °C). In other words, the peak hardness is observed at the border between regions [II] and [III]. On the other hand, at aging temperatures above 973 K (700 °C), peak hardness is achieved after the nucleation of needle-shaped β' -Cu₄Ti precipitates at the border between regions [I] and [II]. The features observed at high aging temperatures are most likely associated with the coarsening of needle-shaped β' -Cu₄Ti precipitates *via* Ostwald growing and hence decreasing the number density, which is promoted by the prominent bulk diffusion at high temperatures.

Considering the balance between the electrical conductivity and hardness, the TTT diagram depicted in Figure 12 describes the aging conditions, under which both the parameters increase, as regions [I] and [II]; those, under which electrical conductivity increases, but hardness decreases, as region [III]; and those, under which both the electrical conductivity and hardness remain constant, as region [IV]. Thus, the revised TTT diagram demonstrates that the low-temperature aging process (below 693 K (420 °C)) can increase the electrical conductivity of peak-hardened specimens up to the values exceeding 15 pct IACS and also reveals that low-temperature aging is not so practical since it takes a long period of more than 2880 minutes (48 hours). In order to enhance alloy properties efficiently,

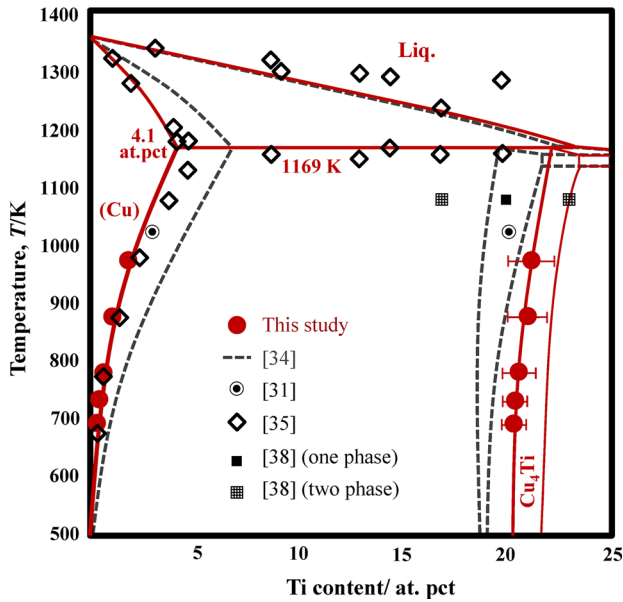


Fig. 10—A Cu-rich portion of the Cu-Ti binary partial phase diagram proposed in this study, which is depicted by the solid lines. The solid circles represent the experimental data obtained by IC-P-OES after extraction, which are listed in Table II. The dotted lines are cited from the recent phase diagram reported by Turchanin *et al.*^[34] Symbols show experimental data from Refs. [31,35,38].

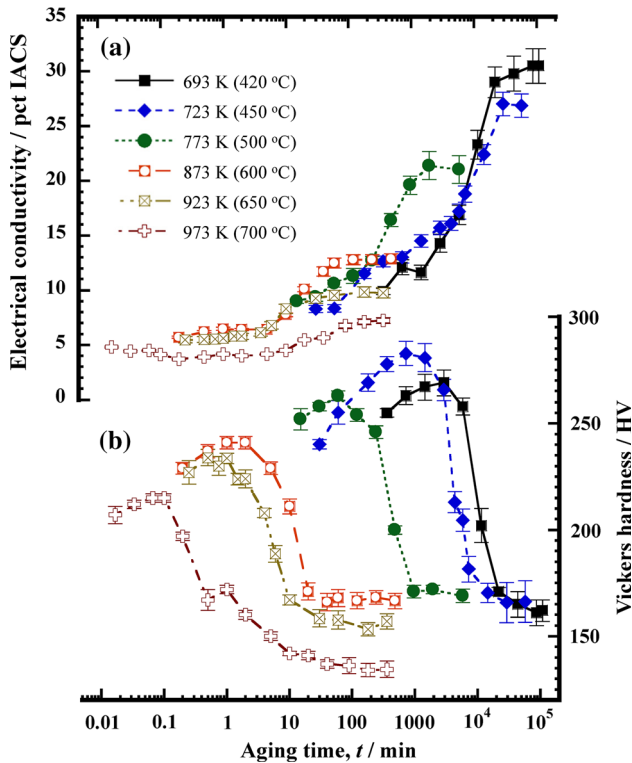


Fig. 11—(a) Electrical conductivity and (b) hardness values for the Cu-4 at. pct Ti alloy specimens aged between 693 K (420 °C) and 973 K (700 °C).

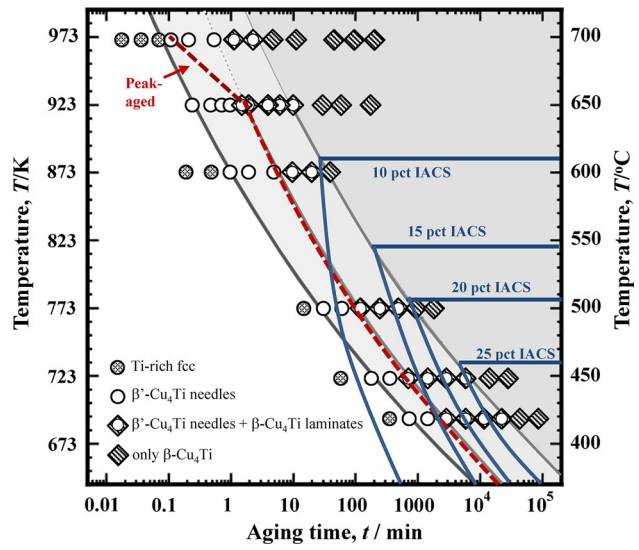


Fig. 12—Aging conditions drawn on the TTT diagram for the peak aged and fully aged Cu-4 at. pct Ti alloy specimens, which resulted in an increase in the alloy electrical conductivity from 10 to 25 pct IACS.

its microstructure must be controlled either through the addition of various elements or by utilizing other techniques such as prior deformation, multiple heat treatment cycles, and thermodynamic procedures.

IV. CONCLUSIONS

The kinetics and phase equilibrium of the microstructural evolution of Cu-4 at. pct Ti alloy during isothermal aging in the temperature region between 693 K (420 °C) to 973 K (700 °C) have been systematically investigated in this study. The obtained findings can be summarized as follows:

- (1) The microstructural evolution of the specimens isothermally aged at temperatures between 693 K (420 °C) and 973 K (700 °C) progressed in accordance with the following sequence: compositional modulation due to spinodal decomposition, continuous precipitation of the needle-shaped metastable β' -Cu₄Ti species with a tetragonal structure, discontinuous precipitation of the cellular components containing the lamellar stable β -Cu₄Ti species with an orthorhombic structure, and precipitation saturation in the equilibrium state. For the specimens aged below 923 K (650 °C), the formation of the stable β -Cu₄Ti phase is limited by the cellular reaction at the grain boundaries, which leads to the ultimate occupation by the cellular components in the specimens during the final aging stage. In the case of aging at 973 K (700 °C), both the nucleated stable β -Cu₄Ti species and pre-ex-

isting β' -Cu₄Ti precipitates grow at the grain boundaries (most likely because of the prominent bulk diffusion at high temperatures).

- (2) According to the TTT diagram proposed for Cu-4 at. pct Ti alloy, the kinetics of the β' -Cu₄Ti precipitation initiation, formation of β' -Cu₄Ti species due to cellular reaction, and alloy microstructural equilibrium can be described by Eqs. [1], [2], and [3], respectively. The kinetics of the β' -Cu₄Ti initiation due to cellular reaction corresponds to the aging conditions for achieving alloy peak hardness at temperatures below 923 K (650 °C). The proposed TTT diagram also reveals that low-temperature aging increases the electrical conductivity of peak-hardened specimens up to the values exceeding 15 pct IACS.
- (3) The Cu-rich portion of the Cu-Ti binary phase diagram was revised based on the compositional analysis of the precipitates performed after the extraction procedure. The solidus lines for the α phase of the Cu solid solution and β' -Cu₄Ti precipitates can be described by Eqs. [4] and [5], respectively.

ACKNOWLEDGMENTS

The authors are grateful to Professor S. Hanada and Prof. N. Masahashi from the Institute for Materials Research (IMR) of Tohoku University, Professor Y. Kaneno and Professor T. Matsui from Osaka Prefecture University, and Dr. A. Sugarawa, Dr. F. Sasaki, and Mr. H. Suda from DOWA METALTECH Co., Ltd. for their useful discussions and comments. The authors also thank Dr. M. Nagasako, Dr. M. Ishikuro, Mr. E. Aoyagi, and Mr. S. Ito from IMR for technical assistance. Financial support was provided by the Japan Society for the Promotion of Science in the framework of the Grant-in-Aid for Scientific Research program (Grant No. 26420663) and by the Japan Copper and Brass Association (2016).

REFERENCES

1. R. Knights and P. Wilkers: *Acta Metall.*, 1973, vol. 21, pp. 1503–14.
2. D.E. Laughlin and J.W. Cahn: *Acta Metall.*, 1975, vol. 23, pp. 329–39.
3. Datta and W.A. Soffa: *Acta Metall.*, 1976, vol. 24, pp. 987–1001.
4. A.W. Thompson and J.C. Williams: *Metall. Trans. A*, 1984, vol. 15A, pp. 931–37.
5. P.E. Donovan: *J. Mater. Sci. Lett.*, 1985, vol. 4, pp. 1337–39.
6. W.A. Soffa and D.E. Laughlin: *Acta Metall.*, 1989, vol. 37, pp. 3019–28.
7. S. Nagarjuna, M. Srinivas, K. Balasubramanian, and D.S. Sarma: *Acta Mater.*, 1996, vol. 44, pp. 2285–93.
8. S. Nagarjuna, K. Balasubramanian, and D.S. Sarma: *J. Mater. Sci.*, 1997, vol. 32, pp. 3375–85.
9. A.A. Hamed and L. Blaz: *Mater. Sci. Eng. A*, 1998, vol. 254, pp. 83–89.
10. C. Borchers: *Philos. Mag. A*, 1999, vol. 79, pp. 537–47.
11. S. Nagarjuna and D.S. Sarma: *Scr. Mater.*, 1999, vol. 41, pp. 359–63.
12. W.A. Soffa and D.E. Laughlin: *Prog. Mater. Sci.*, 2004, vol. 49, pp. 347–66.
13. R. Markandeya, S. Nagarjuna, and D.S. Sarma: *Mater. Sci. Eng. A*, 2005, vol. 404, pp. 305–13.
14. S. Nagarjuna and M. Srinivas: *Mater. Sci. Eng. A*, 2005, vol. 406, pp. 186–94.
15. S. Semboshi and T.J. Konno: *J. Mater. Res.*, 2008, vol. 23, pp. 473–77.
16. V. Lebreton, D. Panchoutinski, and Y. Bienvenu: *Mater. Sci. Eng. A*, 2009, vol. 508, pp. 83–92.
17. S. Semboshi, T. Nishida, H. Numakura, and R. Kirchheim: *Metall. Mater. Trans. A*, 2011, vol. 42, pp. 2136–43.
18. L. Si, L. Zhou, X. Zhu, L. Sanhua, S. Leinuo, and D. Qiyi: *Mater. Sci. Eng. A*, 2016, vol. 650, pp. 345–53.
19. S. Semboshi, S. Sato, M. Ishikuro, K. Wagatsuma, A. Iwase, and T. Takasugi: *Metall. Mater. Trans. A*, 2014, vol. 45, pp. 3401–11.
20. L.A. Nesbit and D.E. Laughlin: *Acta Metall.*, 1978, vol. 26, pp. 815–25.
21. S. Sato, A. Hasegawa, S. Semboshi, and K. Wagatsuma: *High Temp. Mater. Processes*, 2015, vol. 34, pp. 123–30.
22. F. Findik: *Mater. Des.*, 2012, vol. 42, pp. 131–46.
23. S. Chen, Y.H. Duan, B. Huang, and W.C. Hu: *Philos. Mag.*, 2015, vol. 95, pp. 3535–53.
24. Y.D. Zhu, M.F. Yan, Y.X. Zhang, and C.S. Zhang: *Comput. Mater. Sci.*, 2016, vol. 123, pp. 70–78.
25. R.C. Ecol, J.V. Bee, and B. Ralph: *Phys. Status Solidi*, 1979, vol. 52A, pp. 201–10.
26. R.C. Ecol, J.V. Bee, and B. Ralph: *Metall. Mater. Trans. A*, 1980, vol. 11A, pp. 1407–14.
27. R.W. Fonda and G.J. Shiflet: *Scr. Metall.*, 1990, vol. 24, pp. 2259–62.
28. R.W. Fonda and G.J. Shiflet: *Metall. Mater. Trans. A*, 2002, vol. 33A, pp. 2507–18.
29. T. Doi: *Acta Metall.*, 1959, vol. 7, pp. 291–92.
30. S. Ikeno, S. Saji, and S. Hori: *J. Japan Inst. Met. Mater.*, 1974, vol. 38, pp. 446–51 (in Japanese).
31. C.R. Hutchinson, R.E. Hackenberg, and G.J. Shiflet: *Ultramicroscopy*, 2003, vol. 94, pp. 37–48.
32. S. Semboshi, M. Ishikuro, S. Sato, K. Wagatsuma, and T. Takasugi: *Mater. Charact.*, 2013, vol. 82, pp. 23–31.
33. C. Bellot and P. Lamesle: *J. Alloys Compd.*, 2013, vol. 570, pp. 100–03.
34. M.A. Turchanin, P.G. Agraval, and A.R. Abdulov: *Powder Metall. Met. Ceram.*, 2008, vol. 47, pp. 344–60.
35. E. Raub, P. Walter, and H. Engel: *Z. Metallkd.*, 1952, vol. 43, pp. 112–18.
36. M.J. Saarivirta and H.S. Cannon: *Met. Prog.*, 1959, vol. 76, pp. 81–84.
37. V.N. Eremenko, Y.I. Buyanov, and S.B. Prima: *Powder Metall. Met. Ceram.*, 1966, vol. 5, pp. 494–502.
38. V.N. Eremenko, Y.I. Buyanov, and N.M. Panchenko: *Powder Metall. Met. Ceram.*, 1970, vol. 9, pp. 410–19.
39. G. Verger, J.M. Pelletier, and J. Merlin: *J. Less-Common Met.*, 1979, vol. 64, pp. 175–83.
40. J.-Y. Brun, S.-J.-H. Thibault, and C.-H. Allibert: *Z. Metallkd.*, 1983, vol. 74, pp. 525–29.
41. N. Karlsson: *J. Inst. Met.*, 1951, vol. 78, pp. 391–405.
42. J. Miyake and M.E. Fine: *Acta Metall.*, 1992, vol. 40, pp. 733–41.
43. S. Suzuki, K. Hirabayashi, H. Shibata, K. Mimura, M. Ishiki, and Y. Waseda: *Scr. Mater.*, 2003, vol. 48, pp. 431–35.
44. R. Landauer: *J. Appl. Phys.*, 1952, vol. 23, pp. 779–84.
45. S. Semboshi, S. Yamauchi, and H. Numakura: *Mater. Trans.*, 2013, vol. 54, pp. 520–27.